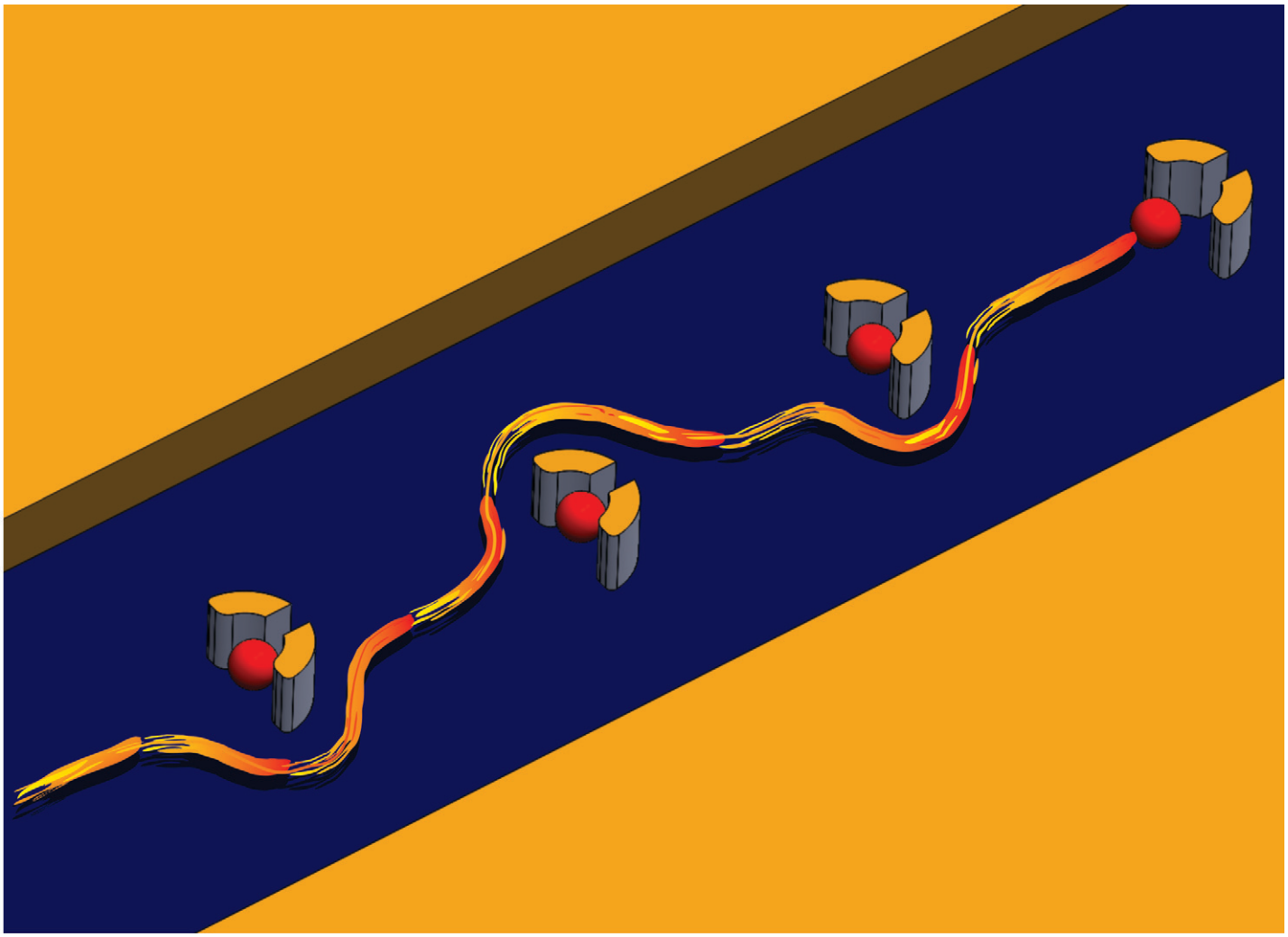

Featuring work from the groups of Dr Marcos at Marcos Research Team (MRT), Nanyang Technological University, Singapore and Dr Raymond H. W. Lam at Laboratory of Advanced Microfluidic Systems (LAMS), City University of Hong Kong.

Deterministic sequential isolation of floating cancer cells under continuous flow

A microfluidic device for deterministic sequential isolation of cells through a series of microsieves with up to 100% trapping yield.

As featured in:

See Marcos, Raymond H. W. Lam *et al.*, *Lab Chip*, 2016, **16**, 2813.

ROYAL SOCIETY OF CHEMISTRY

www.rsc.org/loc

Registered charity number: 207890

Lab on a Chip

PAPER

View Article Online
View Journal | View Issue

Cite this: *Lab Chip*, 2016, **16**, 2813

Deterministic sequential isolation of floating cancer cells under continuous flow†

Quang D. Tran,[a] Tian Fook Kong,[a] Dinglong Hu,[b] Marcos*[a] and Raymond H. W. Lam*[bc]

Received 10th May 2016,
Accepted 28th June 2016

DOI: 10.1039/c6lc00615a

www.rsc.org/loc

Isolation of rare cells, such as circulating tumor cells, has been challenging because of their low abundance and limited timeframes of expressions of relevant cell characteristics. In this work, we devise a novel hydrodynamic mechanism to sequentially trap and isolate floating cells in biosamples. We develop a microfluidic device for the sequential isolation of floating cancer cells through a series of microsieves to obtain up to 100% trapping yield and >95% sequential isolation efficiency. We optimize the trappers' dimensions and locations through both computational and experimental analyses using microbeads and cells. Furthermore, we investigated the functional range of flow rates for effective sequential cell isolation by taking the cell deformability into account. We verify the cell isolation ability using the human breast cancer cell line MDA-MB-231 with perfect agreement with the microbead results. The viability of the isolated cells can be maintained for direct identification of any cell characteristics within the device. We further demonstrate that this device can be applied to isolate the largest particles from a sample containing multiple sizes of particles, revealing its possible applicability in isolation of circulating tumor cells in cancer patients' blood. Our study provides a promising sequential cell isolation strategy with high potential for rapid detection and analysis of general floating cells, including circulating tumor cells and other rare cell types.

Introduction

Microfluidics has been proven to be ideal for achieving a wide range of biological/clinical applications.[1] In particular, isolation and detection of floating cells in liquid biopsy[2] and the following single-cell analysis are made possible with the advancement in microfluidics technology. The main concerns in single-cell isolation lie in obtaining a high capture efficiency and high-level of statistical confidence. Low cell capture efficiency warrants a large sample volume, which in turn increases the sample processing time. On the other hand, increasing the flow rate induces higher shear stress, which adversely affects the structural integrity of the cell membrane and significantly impacts the cell viability.[3] For instance, detection of rare cells is very challenging due to its low abundance nature,[4] in the order of ~1–100 circulating tumor cells (CTCs) per 10^9 blood cells.[5] Therefore, the primary focus of this research is on the realization of a rapid, sensitive, robust, and microfluidic single-cell isolation device.

Over the past few decades, many microfluidic methods have been developed to sort cells based on the dissimilarity in cell properties,[6] which can be identified by immunochemical markers associated with different fluorescence[7] or magnetic[8] signals, and the interactions with the environment based on the intrinsic biophysical properties.[9] Although immunochemical methods provide very promising and specific cell identification, the addition of fluorescence signals would alter cell properties. Further cell manipulation schemes with external forces[10,11] are often required which induce technical challenges for both device operation and system automation. On the other hand, some sorting schemes consider biophysical properties as the natural biomarkers describing cell conditions.[4,12] Dielectrophoretic cell sorting techniques apply the natural differences in the dielectric constant of cell bodies, yet the external electrical field may trigger cell responses and alterations.[13] Many hydrodynamic (size, density, deformability and morphology) techniques and related theories have also been developed for effective implementation of cell sorting.[6,14]

Inertia-based hydrodynamic cell isolation methods, such as trapping of cells using microvortices through a series of expansion reservoirs, have fast processing time. However, the method suffers from a low isolation efficiency of

[a] *School of Mechanical and Aerospace Engineering, Nanyang Technological University, Singapore. E-mail: marcos@ntu.edu.sg; Tel: +65 67905713*
[b] *Department of Mechanical and Biomedical Engineering, City University of Hong Kong, Hong Kong, China. E-mail: rhwlam@cityu.edu.hk; Fax: +852 3442 0172; Tel: +852 3442 8577*
[c] *City University of Hong Kong Shenzhen Research Institute, Shenzhen, China*
† Electronic supplementary information (ESI) available. See DOI: 10.1039/c6lc00615a

approximately 65%.[15] On the other hand, separation of CTCs from blood with a spiral microchannel where the Dean flow fractionation results in inherent centrifugal forces for the migration of cancer cells achieved a higher cell retrieval efficiency of approximately 85%.[5] Nevertheless, the fast movement of cells during the inertial trapping process makes it unable to track single cells, which is vital in some rare cell isolation assays. More recently, a higher cell capture efficiency of ~90–95% was achieved with a microfluidic device with a conical-shaped microfilter.[16] However, while cell trapping through an array of microfilters takes delight in higher cell isolation efficiency, the method essentially employs a strategy of scouting for the cells *via* a "big fishing net", and thus require considerable effort in locating the trapped cells in random positions of the vast array of microtrappers.[17] Additionally, acoustic waves can be applied to achieve high-throughput separation of cells with different physical properties including size, density and compressibility combined as an acoustic radiation force pulling the cells aside to the collection outlet.[18] It has also been reported that the cell size and deformation under hydrodynamic stretching at an inertial focusing position can be observed by an automated microscope installed with a high-speed image processing system.[19] Altogether, there remains a need for a cell isolation device that is capable of achieving high isolation efficiency, and with easily traceable cell positions.

In this work, we develop a lab-on-a-chip microfluidic device for label-free rapid single-cell isolation through a series of microsieves with up to 100% trapping yield and >95% sequential isolation efficiency. These trappers comprise semicircular arcs spaced at specific offsets and distance apart. We introduce two offset parameters in the sieve design – the 'initial offset' and 'sieve offset', to dictate the desired trajectories of the cells for efficient sequential trapping. As a proof-of-concept for the effectiveness of the novel microsieve design for cell isolation, we performed a series of parametric studies to investigate the trapping characteristics of polystyrene microbeads, and subsequently a human breast cancer cell line. With the proposed design and framework of the innovative sequential cell isolation device, we are able to precisely isolate floating cells at pre-determined positions of the device, thus eliminating the need for exhaustive search and recovery effort required by other physical large-array microstructure trapper schemes for identifying the location of trapped cells. Furthermore, due to the position specificity and consistent physical conditions of cells in the microsieves, we are able to provide a robust platform for unprecedented single cell handling for subsequent fundamental studies and clinical analysis, such as the investigation of effects of new drugs, rare cell heterogeneity, and cell monitoring.

Theory and device design

Working principle

The microfluidic device for sequential isolation of floating cancer cells comprises a series of microsieves positioned at

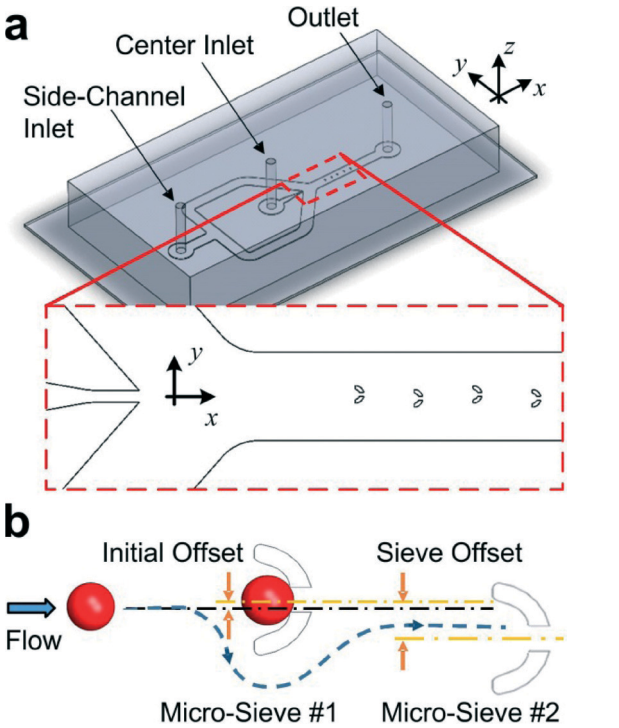

Fig. 1 (a) Design of the sequential isolation microdevice for floating cells. (b) Configuration of the microsieve positions. With the lateral 'initial offset' from the center of the flow channel, the first floating cell be trapped in the first sieve, and the second cell would predominantly bypass through the negative *y*-side of the first sieve and be trapped at the second sieve position with a lateral 'sieve offset'.

defined locations along the continuous flow stream as described in Fig. 1a. The novel arrangement of the microsieves enables the trapping of the floating cells in a deterministic and sequential manner. The sample solution is injected to the center inlet, while the buffer flows into the microchannel through the side-channel inlet, which splits into two streams and sandwiches the sample flow as they progress downstream. As such, the cells would be focused along the axial center of the microchannel. The width of the flow coming out from the center inlet can be accurately controlled by adjusting the flow rate ratio between the two inlets.[20,21] For example, if the side inlet flow rate is Q_s and the center inlet flow rate is Q_c, due to mass conservation, the width of the center flow would occupy $Q_c/(Q_s + Q_c)$ of the total channel width. Thus, the cells in the sample solution will be hydrodynamically focused towards the axial center of the microchannel if $Q_s \gg Q_c$.

In low Reynolds number flows (Stokes flow), the inertial effect is negligible and the flow field in the microchannel is well defined.[22,23] When a cell enters the microchannel, its trajectory follows the streamline under the laminar regime[24,25] and encounters the array of microsieves. Each microsieve comprises a semicircular-arc structure with an opening at its center located along the flow channel, with precisely defined lateral offsets (along the *y*-direction) and separation distance (along the *x*-direction) between the

microsieves. The cell, with physical dimensions larger than the opening of the microsieve, will be trapped at the microsieve if the streamline passes through the opening. The geometry of the microsieve structures can be optimized for isolation of cells within a workable range of diameters.

In order to preferentially deflect the trajectory of the subsequent cells after the first microsieve is filled, we introduce a lateral 'initial offset' from the center of the microchannel in the positive *y*-direction (Fig. 1b). The 'initial offset' should be small enough such that the first cell's streamline would still pass through the sieve opening and the cell would be trapped in the first microsieve. The second incoming cell would bypass through the negative *y*-direction of the first sieve due to the aforementioned offset. Subsequently, we introduce another lateral offset, known as the 'sieve offset' to the second microsieve such that the second incoming cell trajectory passes through the sieve opening of the second sieve for the isolation of the second cell. The 'sieve offset' simply represents the lateral distance between the axis of symmetry of the first and second sieves. Note that the sieve offset needs to be larger than the initial offset but smaller than the outer radius of the sieve, such that the third incoming cell, after bypassing the second microsieve, will move to the positive *y*-direction and encounter the third microsieve.

The positioning of the third and fourth sieves is a repeat of the first and second sieves. The number of sieves can be increased up to the total number of desired number of cells isolated using the mentioned pattern. In this work, we demonstrate sequential isolation of beads and cells with a total of 50 microsieves. The microsieve lateral offsets – 'initial offset' and 'sieve offset' – are varied in search for the optimal trapping efficiency. As the flow conditions are well defined at low Reynolds number, the microfluidic device can achieve high-yield, high-repeatability cell isolation at defined positions.

Simulation study

We performed numerical simulations to optimize the sieve separation distance by calculating the flow field around a microsieve trapped with a particle, located in the middle of a straight channel. In the absence of the microsieve, the flow everywhere in the channel is unidirectional. The presence of a microsieve forces the upstream unidirectional streamlines to bend around the sieve and the flow becomes unidirectional again further downstream. The unidirectionality of the flow at any arbitrary location (x, y, z) can be quantified by introducing a dimensionless unidirectional factor, $\varepsilon_V(x,y,z) = \sqrt{(v^2+w^2)/(u^2+v^2+w^2)}$, where the velocity components u, v, w are in the x, y and z directions, respectively. When the flow field is only in the x-direction, v and w are zero, and thus the dimensionless unidirectional factor, $\varepsilon_V = 0$. On the other hand, a non-zero ε_V corresponds to a non-unidirectional flow field. We define x_{sieve} as the reference x position measured from the center of the microsieve (Fig. 2, left). We calculated the average ε_V over the cross section area, $\bar{\varepsilon}_V(x_{sieve}) = \iint \varepsilon_V(x_{sieve}, y, z)\,dy dz \Big/ \iint dy dz$ (Fig. 2 right). The result indicates that a separation of >500 μm can ensure the flow to recover unidirectionally where $\bar{\varepsilon}_V(x_{sieve}) < 0.005$. Therefore, the second microsieve has to be located at least 500 μm downstream from the first one.

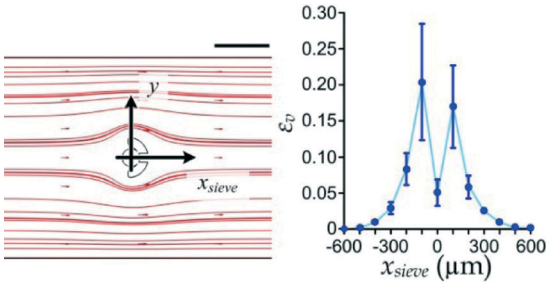

Fig. 2 Velocity profile at the mid-height plane around a microsieve structure at a flow rate of 100 μL min^{-1} (left) and dimensionless unidirectional factor ε_V as a function of x_{sieve} (right). Scale bar: 200 μm. Error bars are standard deviations.

Materials and methods

Device fabrication

We transferred the design of the microfluidic sequential trapper drawn with AutoCAD (Autodesk, USA) to a chrome mask for microfabrication of a negative silicon mold. The mold is fabricated with standard cleanroom photolithography and deep-reactive-ion-etching (DRIE). DRIE was necessary because of the high aspect ratio of the trapper microstructures. The mold was surface-treated by oxygen plasma activation (energy: 5 kJ; Harrick plasma cleaner PDC-002) and deposition of a molecular monolayer of trichloro(1*H*,1*H*,2*H*,2*H*-perfluorooctyl)silane (Sigma-Aldrich, St. Louis, MO). This is to facilitate the release of the cross-linked PDMS (Sylgard 184, Dow Chemical, Midland, MI, USA) from the silicon master. The PDMS substrate was fabricated by the two-stage replica molding technique.[26–29] After peeling off the PDMS substrates from the mold, holes were punched (Harris-Unicore Inc., USA) at the inlets and outlets for liquid accessibility. The substrate was then bonded onto a glass slide using oxygen plasma treatment (energy: 10 kJ). We coated the inner surfaces of the bonded microchannels with 6% bovine serum albumin in phosphate buffered saline (PBS; Sigma Aldrich) to minimize the adhesion between cells and channel walls.

Cell preparation

The MDA-MB-231 human breast cancer cell line (ATCC, Manassas, VA) was cultured in DMEM-12 medium containing 10% fetal bovine serum and 1% penicillin (Life Technologies, Singapore). The cells were maintained at 37 °C with 5% CO_2 supply, with refreshment of the culture media every day. Once a 90% confluent cell population is obtained, cell passage was performed with 0.25% trypsin–EDTA (Life Technologies).

Microbead and cell isolation experimental setup

First, we validated the sequential cell isolation concept using the 'enlarged' device to demonstrate the isolation of 80 μm diameter polystyrene microbeads. The device consists of 50 identical microsieves (inner diameter: 100 μm; outer diameter: 140 μm; gap width: 40 μm) located along the flow channel (width: 900 μm; height: 120 μm) of the device. Subsequently, the dimension of the microfluidic device is scaled down by a factor of four to establish the 'true-scale' isolation device with a sieve opening of 10 μm for isolation of 20 μm diameter polystyrene microbeads and cancer cells.

For the microbead isolation experiments with the 'enlarged device', we prepared the microbead sample by diluting a stock solution of 80 μm diameter polystyrene beads (Duke 4k, Fisher Scientific, Pittsburgh, PA, USA) down to a bead density of 3×10^3 beads per mL. We injected water as a buffer through the side-channel inlet at 10 μl min^{-1}, while clamping the tubing of the center inlet and outlet ports for approximately 3 minutes, to remove the trapped air bubbles. Once all bubbles disappeared, we removed the clamps and injected the sample to the center inlet of the trapper device at a flow rate of 2 μl min^{-1} with a syringe pump (NE-1002X, New Era Pump Systems, Farmingdale, NY). At the same time, we injected water as a buffer to the side inlet of the device at a flow rate of 40 μL min^{-1}. The sample flow was sandwiched by the side buffers, and focused along the axial center of the microchannel. The trapping process was recorded using a high speed camera (Axiocam 506 Color, Zeiss, Jena, Germany) installed to an inverted microscope (Axio Observer.Z1, Zeiss). The experiments ended when all microsieves were filled with the polystyrene beads which occurred in approximately 5–10 minutes.

Similarly, for the validation of the 'true-scale' sequential microtrapper, we conducted the isolation experiment with 20 μm fluorescent microbeads (cat# FP-20052-5, Spherotech, Lake Forest, IL, USA) and MDA-MB-231 human breast cancer cells. The experimental procedures were the same as previously described for the 'enlarged device' experiments, with flow rates of 2 μl min^{-1} and 40 μl min^{-1} for the bead sample and side liquid (water), respectively. For the breast cancer cell isolation experiments, the sample solution was prepared by harvesting MDA cells using 0.25% trypsin–EDTA (Life Technologies) and diluting the cells to a density of 5×10^4 cells per mL in culture media.

Cell viability test

After the sequential cell isolation experiment at a continuous flow rate of 3 μL min^{-1} for 30 min, the sample solution was replaced with reagents of the LIVE/DEAD Cell Viability kit (cat# L-3224, Life Technologies) with a continuous flow from both the sample inlet (flow rate: 0.1 μL min^{-1}) and buffer inlet (flow rate: 2 μL min^{-1}) to stain different fluorescence signals for live and dead cells. The flow of the staining solution was maintained for 20 min, followed by replacing the solution with water for capturing fluorescence images (Axiocam 506 Color, Zeiss, Jena, Germany) using an inverted fluorescence microscope (Axio Observer.Z1, Zeiss).

Flow profile simulation

We applied the simulation software COMSOL Multiphysics (COMSOL, Burlington, MA) to quantify the stabilized streamlines and local velocities of a microchannel section containing a microsieve structure. The total flow rate was set to 100 μL min^{-1}. We adopted the dimensions of the 'enlarged device' for the numerical simulation.

Results and discussion

Concept validation using microbeads

We validated with experiments, for the isolation of 80 μm beads, that an initial offset of 15 μm in the positive *y*-direction could achieve isolation of the first microbead, while deflecting the flow path of the subsequent incoming beads to the intended trajectory through the first sieve in the negative *y*-direction (data not shown). As a proof-of-concept, we first configured the sieve offset to be 45 μm and performed the bead isolation experiment. The key snapshots of the sequential isolation are shown in Fig. 3a (a sample video, Video S1, is also available in the ESI†). This result

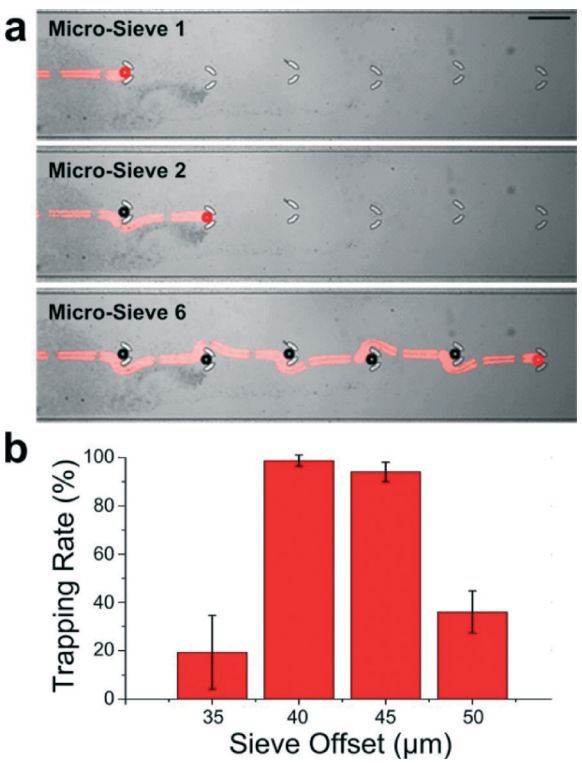

Fig. 3 (a) Sequential isolation process of microbeads. The first bead that enters was trapped in microsieve 1; subsequently the second bead bypassed the first filled trapper and was trapped in microsieve 2. This process continued until all the trappers are filled in a sequential manner. Trace of the bead movements was highlighted in *red*. Scale bar: 200 μm. (b) Trapping rate as a function of sieve offset for the 'enlarged device'. Error bars are standard deviations. $N \geq 5$.

demonstrates the feasibility of our sequential isolation strategy.

We performed a parametric study to characterize the trapping rate as a function of the 'sieve offset' ranging from 35 μm to 50 μm (Fig. 3b). The trapping rate is defined as the percentage of cells flowing into the device isolated in the correct sequence. Our results show that the 'sieve offset' of 40 μm can achieve the highest trapping rate of ~98% for microbeads with a diameter of 80 μm.

Having demonstrated the sequential isolation concept using the larger microbeads of 80 μm, we proceeded to fabricate and test the sequential isolation of 20 μm diameter microbeads using the 'true-scale' microdevice by scaling down the model device with a 4 : 1 geometric ratio (*i.e.* channel width: 225 μm, channel height: 30 μm, inner sieve diameter: 25 μm, outer sieve diameter: 35 μm; sieve gap width: 10 μm, initial offset: 3.75 μm, sieve offset: 10 μm and separation distance: 150 μm). The results (Fig. S2 and Video S2†) indicate an effective sequential isolation using this device with a similar trapping rate (≥96%).

Isolation of size variant microbeads

We further applied the device to examine the feasibility of sequential isolation of a mixture containing microbeads of different sizes. We prepared two mixture samples by mixing 80 μm beads (3×10^3 beads per mL) with 20 μm beads (3×10^4 beads per mL) and 8 μm beads (10^6 cells per mL), respectively; the representative micrographs of the cell isolation are shown in Fig. 4. These results indicate that all the 80 μm beads in the mixture samples were captured in the microsieves while all the smaller microbeads flow to the outlet without being trapped by the microsieve structures. Therefore, the presence of smaller microbeads would not induce significant flow variations large enough to affect the trajectories of the 80 μm beads, thus not impacting the isolation performance of the larger particles. Notably, the diameter of CTCs is typically 15–25 μm,[30] red blood cells has an effective diameter of 5–6 μm (as the major diameter is 6–8 μm and the thickness is ~3 μm)[31] and the diameter of platelets is 2–3 μm.[32] On the other hand, approximately 95% of leukocytes have dimensions less than 15 μm (neutrophil ~62%, 10–14 μm; eosinophil ~2.3% 10–14 μm; basophil ~0.4% 10–14 μm; lymphocyte ~30% 8–10 μm; and monocyte ~5.3% 15–20 μm).[33] Thus, the proposed sequential isolation scheme is applicable to extract CTCs from a blood sample containing abundant red blood cells, platelets, and the majority of white blood cells. The small amount of white blood cells trapped can be further differentiated from the CTCs through on-chip fluorescence immunostaining,[5] fluorescence-activated cell sorting (FACS),[34] or immunomagnetic separation,[34] or density gradient centrifugation.[35]

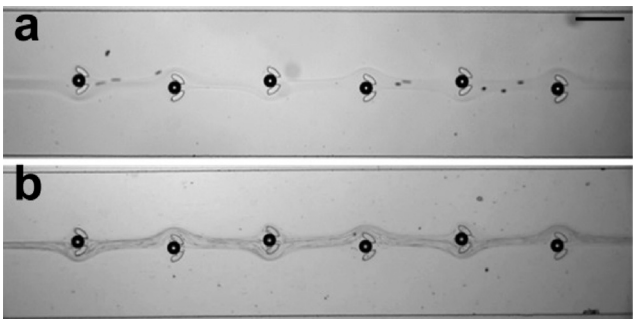

Fig. 4 Isolation of 80 μm microbeads from (a) the mixture of 80 μm beads and 20 μm beads, and (b) the mixture of 80 μm beads and 8 μm beads, implemented on the enlarged device. Scale bar: 200 μm.

Sequential cancer cell isolation

Unlike rigid microbeads, live cells are deformable in the microsieves under hydrodynamic pressure, and such deformation is time-dependent due to the cell viscoelasticity.[36,37] Therefore, it is necessary to investigate the allowable flow rate and duration for successful live-cell encapsulation. We performed sequential isolation experiments of human breast cancer cells (MDA-MB-231) using the 'true-scale' microdevice under different sample flow rates (3 μL min^{-1}, 6 μL min^{-1} and 9 μL min^{-1}). We configured the buffer flow rates to be 20 times the sample flows, adopting the same volumetric ratios as the 'enlarged' device. Here, we consider the encapsulated cell remaining in the microsieve for more than 30 min as a successful isolation. Our results (Fig. 5a) show that the sample flow rate of 3 μL min^{-1} achieved the required isolation, whereas the flow rate of 9 μL min^{-1} was clearly beyond the workable pressure range. The flow rate of 6 μL min^{-1} induced an unfavorable cell condition after 30 min, where the cell body stayed partially outside the microsieve. This indicates that the microsieve gap was likely to squeeze the inner cellular structures including the nucleus.

We characterize the cell trapping rate of MDA-MB-231 for different sieve offsets, ranging from 9 μm to 11 μm (with steps of 0.5 μm) under the sample flow rate of 3 μL min^{-1} and the buffer flow rate of 60 μL min^{-1}, with the procedures described in Methods. The isolation performance of the 'true-scale' device (Fig. 5b) perfectly agrees with the 'enlarged device' (Fig. 2c). The 'enlarged device' has an optimal sieve offset of 40 μm with a trapping efficiency of ~98%, while the scaled down 'true scale' device with a 4 : 1 geometric ratio has an optimal sieve offset of 10 μm with the highest cell trapping efficiency of ~90%. Occasionally, we observed that a few cells were not trapped in the device in sequence. This could be due to a suboptimal sieve offset and other factors including the Brownian motion effect of microparticles and the pressure fluctuations generated in the syringe pump. The trapping rate represents the percentage of cell isolation in the correct sequence. The escaped cells are recaptured in the following microsieves downstream in the device. The total number of microsieves for the 'true-scale' device is 50.

Furthermore, we examined the effect of continuous flow in the microfluidic isolation on the cell viability by examining the ratios of live/dead cells before injection and after

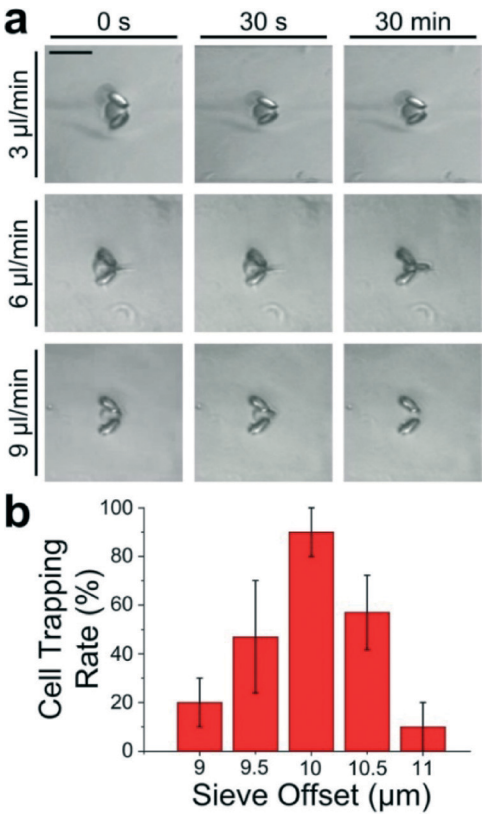

Fig. 5 (a) Microscopic snapshots of cells trapped in 'true-scale' microsieves for different durations of encapsulation (0 s, 30 s and 30 min) under different sample flow rates (3 μL min^{-1}, 6 μL min^{-1} and 9 μL min^{-1}). Scale bar: 50 μm. (b) Trapping rate of cancer cells MDA-MB-231 as a function of the sieve offset, ranging from 9–11 μm. Error bars are standard deviations. $N \geq 5$.

isolation (under a continuous flow of ≥30 min) in the microdevice (both included ~100% of live cells in populations). Fig. 6 shows the representative bright-field and fluorescence micrographs of MDA cells after treatment of the live/dead cell viability assay. We observed that the sequential cell isolation does not affect the cell viability. It has been reported by Barnes *et al.* that ~100% viability of cancer cells can be maintained for shear stress <100 dyne cm^{-2},[38,39] which agrees perfectly with the cell viability result in the sequential isolation microdevice with induced shear stresses on trapped cells in the scale of ~3.7 dyne cm^{-2} (considering the average flow velocity was ~11.1 mm s^{-1} and the characteristic length was the channel height 30 μm). More importantly, the microdevice can provide a unique advantage of knowing the predefined cell positions after isolation, implying that efforts for scanning and cell monitoring operations can be largely reduced. For instance, microscopic images of the trapped cells can be obtained by scanning along the microsieve positions in sequence. The cell viability test has also demonstrated the compatibility of this microdevice in general cell analysis applications, including drug treatments and specific staining techniques.[40]

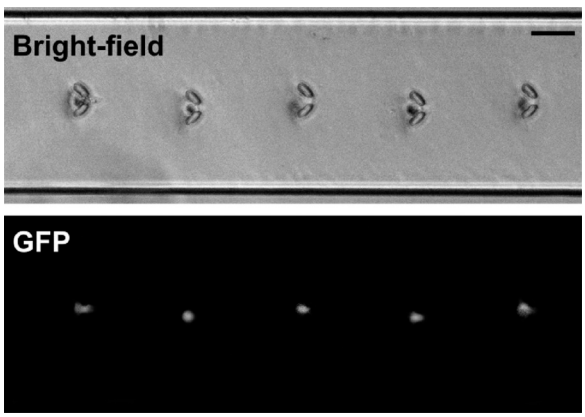

Fig. 6 Representative bright-field (upper) and fluorescence (lower) microscopic images of MDA cells after treatment of the live/dead cell viability assay. The presence of fluorescence signals for all the trapped cells indicates their viability. Scale bar: 50 μm.

Alternative continuous-flow particle focusing techniques based on acoustic[41] or physical[42] effects can be further integrated with the sequential isolation scheme reported here such that no side buffer flow is required and the throughput of each of the microdevices can be increased to ~63 μL min^{-1}. The cell isolation throughput can be further enhanced by pumping the sample into the multiple (around 5–10) microdevices working in parallel, in order to reach the required standard blood processing volume (≥7.5 mL) within a manageable timeframe of ~1 h.[43]

Conclusions

In summary, we have developed an innovative sequential cell isolation device with up to 100% isolation yield and >95% sequential isolation efficiency through a series of microsieves arranged in a novel arrangement. By applying a constant sample flow rate through a microchannel, particles or cells are trapped automatically and sequentially in the microsieves at precisely defined positions. With the low Reynolds number laminar flow used in the microfluidic channel, the structural integrity of the cell membrane, cell viability and genome in the nucleus remain intact and ready for subsequent detection and analysis. Furthermore, the throughput of the system can be substantially increased with the parallelization of the microtrapper design, reducing the processing time to approximately 10 minutes. The reported framework of sequential cell isolation microstructures offers a robust platform for isolation of floating cells in biosamples, and also provide a fitting platform for fundamental studies and clinical applications, such as the investigation of tumor drug resistance and tumor heterogeneity, and demonstration of on-chip single cell labelling and viability tests.

Acknowledgements

We acknowledge financial support from the National Natural Science Foundation of China (NSFC 31500758) and the City University of Hong Kong (SG 7003019).

References

1 E. K. Sackmann, A. L. Fulton and D. J. Beebe, *Nature*, 2014, **507**, 181–189.
2 M. Ilie, V. Hofman, E. Long, O. Bordone, E. Selva, K. Washetine, C. H. Marquette and P. Hofman, *Ann. Transl. Med.*, 2014, **2**(11), 107.
3 J. P. Smith, A. C. Barbati, S. M. Santana, J. P. Gleghorn and B. J. Kirby, *Electrophoresis*, 2012, **33**, 3133–3142.
4 Y. Chen, P. Li, P. H. Huang, Y. Xie, J. D. Mai, L. Wang, N. T. Nguyen and T. J. Huang, *Lab Chip*, 2014, **14**, 626–645.
5 H. W. Hou, M. E. Warkiani, B. L. Khoo, Z. R. Li, R. A. Soo, D. S. W. Tan, W. T. Lim, J. Han, A. A. S. Bhagat and C. T. Lim, *Sci. Rep.*, 2013, **3**, 1259.
6 P. Sajeesh and A. K. Sen, *Microfluid. Nanofluid.*, 2014, **17**, 1–52.
7 J.-C. Baret, O. J. Miller, V. Taly, M. Ryckelynck, A. El-Harrak, L. Frenz, C. Rick, M. L. Samuels, J. B. Hutchison and J. J. Agresti, *Lab Chip*, 2009, **9**, 1850–1858.
8 K. E. McCloskey, L. R. Moore, M. Hoyos, A. Rodriguez, J. J. Chalmers and M. Zborowski, *Biotechnol. Prog.*, 2003, **19**, 899–907.
9 D. R. Gossett, W. M. Weaver, A. J. Mach, S. C. Hur, H. T. K. Tse, W. Lee, H. Amini and D. Di Carlo, *Anal. Bioanal. Chem.*, 2010, **397**, 3249–3267.
10 P. Chen, X. Feng, R. Hu, J. Sun, W. Du and B.-F. Liu, *Anal. Chim. Acta*, 2010, **663**, 1–6.
11 X. Wang, S. Chen, M. Kong, Z. Wang, K. D. Costa, R. A. Li and D. Sun, *Lab Chip*, 2011, **11**, 3656–3662.
12 T. F. Kong, W. Ye, W. K. Peng, H. W. Hou, Marcos, P. R. Preiser, N. T. Nguyen and J. Han, *Sci. Rep.*, 2015, **5**, 11425.
13 G. Mernier, N. Piacentini, T. Braschler, N. Demierre and P. Renaud, *Lab Chip*, 2010, **10**, 2077–2082.
14 M. Chabert and J.-L. Viovy, *Proc. Natl. Acad. Sci. U. S. A.*, 2008, **105**, 3191–3196.
15 M. Dhar, J. Wong, A. Karimi, J. Che, C. Renier, M. Matsumoto, M. Triboulet, E. B. Garon, J. W. Goldman, M. B. Rettig, S. S. Jeffrey, R. P. Kulkarni, E. Sollier and D. Di Carlo, *Biomicrofluidics*, 2015, **9**, 064116.
16 Y. Tang, J. Shi, S. Li, L. Wang, Y. E. Cayre and Y. Chen, *Sci. Rep.*, 2014, **4**, 6052.
17 W. Chen, N. T. Huang, B. Oh, R. H. Lam, R. Fan, T. T. Cornell, T. P. Shanley, K. Kurabayashi and J. Fu, *Adv. Healthcare Mater.*, 2013, **2**, 965–975.
18 P. Li, Z. Mao, Z. Peng, L. Zhou, Y. Chen, P.-H. Huang, C. I. Truica, J. J. Drabick, W. S. El-Deiry and M. Dao, *Proc. Natl. Acad. Sci. U. S. A.*, 2015, **112**, 4970–4975.
19 D. R. Gossett, T. Henry, S. A. Lee, Y. Ying, A. G. Lindgren, O. O. Yang, J. Rao, A. T. Clark and D. Di Carlo, *Proc. Natl. Acad. Sci. U. S. A.*, 2012, **109**, 7630–7635.
20 Marcos, H. C. Fu, T. R. Powers and R. Stocker, *Phys. Rev. Lett.*, 2009, **102**, 158103.
21 J. R. Seymour, T. Ahmed, Marcos and R. Stocker, *Limnol. Oceanogr.: Methods*, 2008, **6**, 477–488.
22 Marcos, C. Yang, K. T. Ooi, T. N. Wong and J. H. Masliyah, *J. Colloid Interface Sci.*, 2004, **275**, 679–698.
23 Marcos, C. Yang, T. N. Wong and K. T. Ooi, *Int. J. Eng. Sci.*, 2004, **42**, 1459–1481.
24 A. Guan, A. Shenoy, R. Smith and Z. Li, *Biomicrofluidics*, 2015, **9**, 024103.
25 G. B. Jeffery, *Proc. R. Soc. London, Ser. A*, 1922, **102**, 161–179.
26 R. Pantoja, J. M. Nagarah, D. M. Starace, N. A. Melosh, R. Blunck, F. Bezanilla and J. R. Heath, *Biosens. Bioelectron.*, 2004, **20**, 509–517.
27 M. A. Unger, H. P. Chou, T. Thorsen, A. Scherer and S. R. Quake, *Science*, 2000, **288**, 113–116.
28 G. M. Whitesides, E. Ostuni, S. Takayama, X. Jiang and D. E. Ingber, *Annu. Rev. Biomed. Eng.*, 2001, **3**, 335–373.
29 T. Deng, H. Wu, S. T. Brittain and G. M. Whitesides, *Anal. Chem.*, 2000, **72**, 3176–3180.
30 S. Zheng, H. Lin, J. Q. Liu, M. Balic, R. Datar, R. J. Cote and Y. C. Tai, *J. Chromatogr. A*, 2007, **1162**, 154–161.
31 E. L. Persons, *J. Clin. Invest.*, 1929, **7**, 615.
32 J. M. Paulus, *Blood*, 1975, **46**, 321–336.
33 E. P. Solomon, *Introduction to Human Anatomy and Physiology*, Elsevier Health Sciences, 2015.
34 R. L. Eifler, J. Lind, D. Falkenhagen, V. Weber, M. B. Fischer and R. Zeillinger, *Cytometry, Part B*, 2011, **80**, 100–111.
35 R. Gertler, R. Rosenberg, K. Fuehrer, M. Dahm, H. Nekarda and J. R. Siewert, in *Molecular Staging of Cancer*, ed. H. Allgayer, M. M. Heiss and F. W. Schildberg, Springer Berlin Heidelberg, Berlin, Heidelberg, 2003, DOI: 10.1007/978-3-642-59349-9_13, pp. 149–155.
36 S. Suresh, *Acta Mater.*, 2007, **55**, 3989–4014.
37 V. Swaminathan, K. Mythreye, E. T. O'Brien, A. Berchuck, G. C. Blobe and R. Superfine, *Cancer Res.*, 2011, **71**, 5075–5080.
38 J. M. Barnes, J. T. Nauseef and M. D. Henry, *PLoS One*, 2012, **7**, e50973.
39 R. H. Lam, Y. Sun, W. Chen and J. Fu, *Lab Chip*, 2012, **12**, 1865–1873.
40 Z. Wang, M. C. Kim, M. Marquez and T. Thorsen, *Lab Chip*, 2007, **7**, 740–745.
41 M. E. Piyasena, P. P. Austin Suthanthiraraj, R. W. Applegate Jr, A. M. Goumas, T. A. Woods, G. P. López and S. W. Graves, *Anal. Chem.*, 2012, **84**, 1831–1839.
42 S. Hu, G. Liu, W. Chen, X. Li, W. Lu, R. H. Lam and J. Fu, *Small*, 2016, **12**, 2300–2311.
43 P. Grover, A. Cummins, T. Price, I. Roberts-Thomson and J. Hardingham, *Ann. Oncol.*, 2014, **25**, 1506–1516.